Layer-by-Layer Self-Assembly: Toward Magnetic Films with Tunable Anisotropy

ARTICLE *in* THE JOURNAL OF PHYSICAL CHEMISTRY C · APRIL 2015

Impact Factor: 4.77 · DOI: 10.1021/acs.jpcc.5b01065

7 AUTHORS, INCLUDING:

Yanming Wang
Chinese Academy of Sciences
5 PUBLICATIONS **42** CITATIONS
SEE PROFILE

C. J. Luo
University of Cambridge
13 PUBLICATIONS **351** CITATIONS
SEE PROFILE

M. S. Darwish
Egyptian Petroleum Research Institute
11 PUBLICATIONS **38** CITATIONS
SEE PROFILE

Stoyan K. Smoukov
University of Cambridge
64 PUBLICATIONS **1,574** CITATIONS
SEE PROFILE

THE JOURNAL OF PHYSICAL CHEMISTRY C

Article

pubs.acs.org/JPCC

Layer-by-Layer Self-Assembly: Toward Magnetic Films with Tunable Anisotropy

Wenying Shi,*[,†,‡] Ruizheng Liang,[†] Simin Xu,[†] Yanming Wang,[‡] Chaojie Luo,[‡] Mohamed Darwish,[‡,§] and Stoyan K. Smoukov*[,‡]

[†]State Key Laboratory of Chemical Resource Engineering, Beijing University of Chemical Technology, Beijing 100029, P. R. China
[‡]Department of Materials Science and Metallurgy, University of Cambridge, 27 Charles Babbage Road, Cambridge CB3 0FS, U.K.
[§]Egyptian Petroleum Research Institute, 1 Ahmed El-Zomor Street, El Zohour Region, Nasr city, Cairo 11727, Egypt

Supporting Information

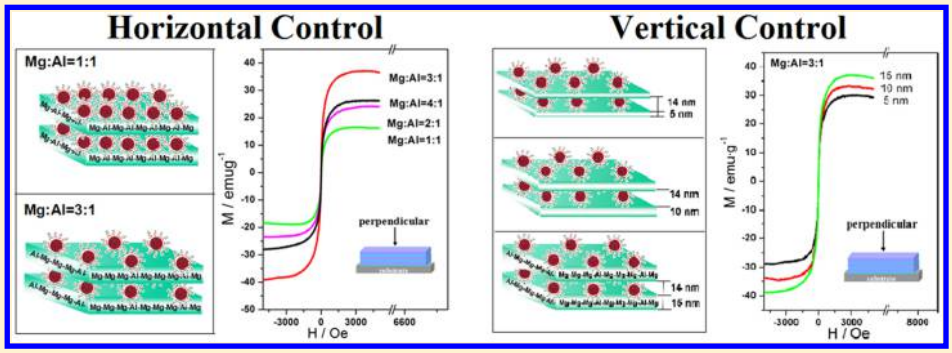

ABSTRACT: Highly anisotropic magnetic films are possible to fabricate by control of the coupling between individual magnetic particles. Selective control over coupling in the horizontal and vertical directions are of both fundamental and practical interest. Here we show such control in the multiple layer-by-layer (LBL) self-assembly of layered double hydroxide (LDH) nanosheets (x = 1, 2, 3 and 4) with thicknesses of 5−15 nm, co-assembled with 3-aminopropyl-trimethoxysilane (APTS) modified spherical Fe_3O_4 nanoparticles (APTS-Fe_3O_4 NPs) on quartz substrates. The electrostatic charge density on the LDH sheets, controlled by the Mg/Al composition ratio, affects the NP packing in a single horizontal layer, while the thickness of the LDH sheets controls magnetic coupling between layers. The tunable magnetic properties (coercivity H_c, saturation magnetization M_s, anisotropy, and blocking temperatures) are measured as a function of these parameters. The maximum saturation magnetizations M_s, 36.3 and 25.1 emu·g^{-1} in the perpendicular and parallel direction, respectively, are found for the sample of x = 3 = Mg/Al ratio in the LDH layer, and 15 nm LDH layer thickness. This work provides a general method to adjust the anisotropy of magnetic films based on directional control of coupling of magnetic nanoparticles between and across, LDH nanosheets. We outline how higher anisotropy and even finer control could be achieved by pH and composition control over the electrostatic charge of the assembly components.

1. INTRODUCTION

The anisotropy of magnetic nanoparticle assemblies, resulting in magnetic hysteresis, has raised considerable attention, since it is required for the building blocks of nanoscale memory cells[1,2] and nontrivial quantum dynamics that are crucial for quantum information processing.[3,4] However, achieving 3D structures with control over magnetic anisotropy from the most common spherical nanoparticle still remains a great challenge because of the need to control spacing and orientation in several directions. Spherical magnetic nanoparticles can be densely packed into patterned templates (e.g., nanotubes, nanoholes, etc.), and by controlling interparticle distances their dipole−dipole interactions can have a great effect on anisotropy.[5−8] Most methods, however, are only effective in controlling the interparticle distance equally in all directions by tuning the diameter and spacing of the particles, or selectively only in 2D by the pattern template on which the particles adsorb. Another common method employed for obtaining magnetic composite 3D structures is the dispersion of magnetic nanoparticles into a polymer matrix, but tunability of the magnetic anisotropy is still hard to achieve because magnetic nanoparticles are often randomly distributed throughout the polymer matrix and interparticle distance is difficult to control.[9] For obtaining spherical nanoparticle assemblies with high and tunable magnetic anisotropy it is highly desirable to have simultaneous, separate control of the interparticle distance in both the horizontal and vertical directions. Layer-by-layer (LBL) assembly methods have been used successfully to fabricate multilayer films of Fe_3O_4 nanoparticles.[10−14] There is still a

Received: February 2, 2015
Revised: April 2, 2015
Published: April 27, 2015

DOI: 10.1021/acs.jpcc.5b01065
J. Phys. Chem. C 2015, 119, 13215−13223

need, however to develop better separate control over the spacing in both the horizontal and vertical directions.

Recently, the intrinsic anisotropy of inorganic nanosheets of layered double hydroxides (LDHs) has attracted strong interest due to their ability to induce optical anisotropy.[15,16] In particular, optical films with high anisotropy fabricated by electrostatic self-assembly of LDH building blocks and optical molecules with highly symmetric structure[17] or encapsulated in micelles can also be obtained.[18] In addition, to their planar structural rigidity, it is easy to synthesize LDH sheets with precise composition and control over their surface electrostatic charge. Inspired by both factors, we hypothesized LBL assemblies of LDH nanosheets and magnetic nanoparticles may result in magnetic materials with highly tunable anisotropy. The rigid and positively charged LDH nanosheets can fix and disperse Fe_3O_4 nanoparticles, avoiding aggregation and enhancing stability; while the controlled charge density and thickness of LDH nanosheets impart the ability for simultaneously tuning the interparticle distance of magnetic nanoparticles in both horizontal and vertical directions.

Here we demonstrate a simple method to fabricate nanocomposite films with high tunability of spacing and magnetic anisotropy. In order to realize the assembly of monodispersed Fe_3O_4 nanoparticles and LDH nanosheets, 3-aminopropyltrimethoxysilane (APTS) was utilized to modify Fe_3O_4 nanoparticles.[19] The APTS-Fe_3O_4/LDH films were obtained by alternate LBL assembly of LDH nanosheets and APTS-Fe_3O_4 nanoparticles on a quartz substrate. SEM and AFM images show that the film surface is continuous and uniform, and UV−vis absorption spectra indicate a stepwise and regular film growth procedure. The magnetic anisotropy of the films can be tuned by controlling the interparticle distance of Fe_3O_4 nanoparticles in the horizontal and vertical directions, through simply varying the charge density and thickness of the LDH layer. Though we only show assembly at pH = 7.5−8 and integer x = Mg/Al ratios, we show the method could be extended with potentially higher control at higher pH-s and non-integer ratios. The method could potentially be used in the fields of magnetic probes, separations and sensors for ions and biomolecules.

2. EXPERIMENTAL SECTION

2.1. Materials. Analytical grade chemicals including $Mg(NO_3)_2{\cdot}6H_2O$, $Al(NO_3)_3{\cdot}9H_2O$, $NH_3{\cdot}H_2O$, H_2SO_4, H_2O_2, NaOH, HCl, formamide, $FeCl_3{\cdot}6H_2O$, $FeCl_2{\cdot}4H_2O$, and 3-aminopropyltrimethoxysilane (APTS) were purchased from Sigma-Aldrich and used without further purification. Deionized and decarbonated water were used in all the experimental processes.

2.2. Preparation of APTS-Fe_3O_4 Nanoparticles. Fe_3O_4 nanoparticles were prepared by coprecipitation of Fe^{2+} and Fe^{3+} in the presence of NaOH.[20,21] A mixture solution of 50 mL of 1 M $FeCl_3{\cdot}6H_2O$, 50 mL of 0.5 M $FeCl_2{\cdot}4H_2O$, and 50 mL of 0.4 M HCl was stirred vigorously under N_2 at 80 °C, and then 250 mL of 0.5 M NaOH was rapidly added. The black color precipitates were obtained and stirring was kept for 1 h at 80 °C. After that, resulting Fe_3O_4 nanoparticles were cooled to room temperature and then rinsing with water several times. The above nanoparticles (0.01 g) were then added into 100 mL of APTS (0.05 moL L^{-1}) solution treated in an ultrasonic water bath for 20 min at room temperature.[22] The APTS-Fe_3O_4 nanoparticles were obtained by mechanical stirring for 5 h, followed by washing with methanol and water, after which 0.01 g of APTS-Fe_3O_4 nanoparticles was dispersed in 10 mL of water with pH = 7.5−8.0 using an ultrasonic water bath to form a stable dispersion of slightly negatively charged nanoparticles (Figure S1). Magnetic separation was employed when washing all of above samples in our work.

2.3. Fabrication of the (APTS-Fe_3O_4/LDH)$_n$ Films. The Mg_xAl-NO_3 LDH (x = 1, 2, 3, and 4) nanosheets were synthesized by the hydrothermal method reported previously.[23] The exfoliated Mg_3Al-NO_3 LDH nanosheets of different thickness were obtained by shaking a 0.1 g of Mg_3Al-NO_3 LDH in 100 mL of formamide solution for different times (0, 5, and 24 h). The cleaned quartz glass substrate was obtained by immersion in concentrated NH_3/30% H_2O_2 (7:3) and concentrated H_2SO_4 for 30 min each. After each procedure, the quartz substrate was rinsed and washed thoroughly with water. The substrate was dipped in a colloidal suspension (0.1 g mL^{-1}) of LDH nanosheets for 10 min followed by washing thoroughly, and then the substrate was treated with a 100 mL of APTS-Fe_3O_4 aqueous solution (0.01 wt %) for another 10 min followed by washing in water. Multilayer (APTS-Fe_3O_4/LDH)$_n$ films were fabricated by alternate deposition of LDH nanosheets and APTS-Fe_3O_4 nanoparticle suspension for n cycles. All of the water used in the rinsing and washing process was with pH = 7.5−8.0.

2.4. Characterizations. UV−vis absorption spectra were recorded (PerkinElmer Lambda 750) in the range from 200 to 800 nm. X-ray powder diffraction (XRD) patterns were measured using a Philips PW1820 diffractometer under the conditions 40 kV, 50 mA, Cu Kα radiation (λ = 0.154 nm) step-scanned with a scanning rate of 0.5°/min and a 2θ angle ranging from 2° to 70°. The morphology was investigated by using a scanning electron microscope (SEM, ZEISS), transmission electron microscope (TEM, JEOL JEM-2100), and atomic force microscope (AFM, Digital Instruments, version 6.12). The starting materials and the assemblies were analyzed by X-ray photoelectron spectroscopy (XPS) with monochromatized Al Kα exciting X-radiation (PHI Quantera SXM) and Raman spectra with a confocal Raman microspectrometer, 514.5 nm of excitation and 0.50 mV laser power (Renishaw Instruments Co. Ltd., RM2000). The field-dependence magnetization measurements were carried out by a vibrating sample magnetometer (VSM, MicroMag 2900/3900) at room temperature, and the calculation of the magnetization value was based on the film weight (subtracting the weight of the substrate). The curves of magnetization vs temperature were recorded with a superconducting quantum interference device (SQUID) magnetometer (Quantum Design, MPMS MultiVu Application, Revision 1.60). For ZFC measurements, the film samples were first cooled from 300 to 10 K in zero field. Then, under the magnetic field of 10 Oe, the magnetization was recorded during heating the sample up to 300 K. On the other hand, for FC measurements, the film samples were cooled from 300 to 10 K under the magnetic field of 10 Oe, and magnetization was measured in the heating regime under the same magnetic field.

3. RESULTS AND DISCUSSION

3.1. Structural and Morphological Characterizations. Figure 1 shows the powder XRD patterns of Mg_xAl-LDHs (x = 1, 2, 3 and 4), Fe_3O_4, APTS-Fe_3O_4, and exfoliated Mg_3Al-LDHs (t = 0, 5, and 24 h). The patterns of Mg_xAl-LDHs (x = 1, 2, 3, and 4) nanosheets can be indexed to a hexagonal lattice (Figure 1A, curves a−d). The two sharp and intense characteristic

DOI: 10.1021/acs.jpcc.5b01065
J. Phys. Chem. C 2015, 119, 13215−13223

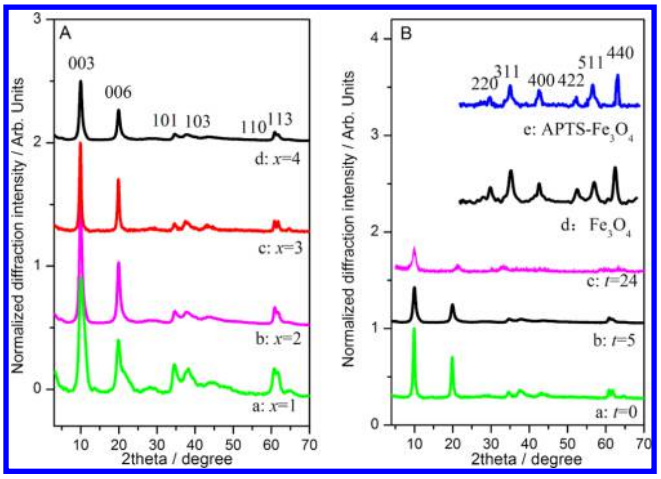

Figure 1. XRD patterns of (A) the Mg_xAl-LDHs (x = 1, 2, 3, and 4) nanosheets and (B) the exfoliated Mg_3Al-LDHs nanosheets (t = 0, 5, and 24 h), Fe_3O_4 nanoparticles, and APTS-Fe_3O_4 nanoparticles. All diffraction intensities were normalized with respect to their corresponding strongest peak.

diffraction peaks appearing as symmetric lines at 2θ 10° and 20° are ascribed to the (003) and (006) plane, consistent with the presence of nitrate as charge compensating anions in the interlayer space. For the exfoliated Mg_3Al-LDHs (t = 0, 5, and 24 h, Figure 1B) nanosheets, the decreased intensity and increased half-peak width (from 0.76° to 0.92°) of the (003) reflection upon prolonging the exfoliated time indicates decreased crystallinity. The diffraction peaks of Fe_3O_4 are indexed a face centered cubic structure (JCPDS No. 65-3107, Figure 1B, curve d).[24] Furthermore, the coated APTS molecule shows no influence on the Fe_3O_4 crystallinity (Figure 1B, curve e).

In order to avoid the effect of LDH nanosheet size on the dispersion degree of APTS-Fe_3O_4 nanoparticles, and directly compare the effects of composition, LDH nanosheets with nearly equal sizes were prepared. TEM images (Figure 2A–D) show the diameter of the Mg_xAl-LDHs (x = 1, 2, 3, and 4) nanosheets is ~100 nm. HRTEM images show the Fe_3O_4 nanoparticles have an average size of ~13 nm, and the particle size distributions are in good agreement with the normal distribution (Figures 2E and 2G, respectively). The HRTEM image shows the clear and continuous lattice fringes (Figure 2F). The lattice fringe pitch of 0.25 nm is magnified and corresponds well with the d-spacing of the (311) reflections for Fe_3O_4, in agreement with the values of 2.53 Å obtained from the JCPDS database.[25] After coating with APTS, the dispersion degree displays an obvious increase because the APTS coating inhibits aggregation of Fe_3O_4 nanoparticles (Figure 2H). The core–shell structure can be observed in the HRTEM image with an average size of 14 nm (Figure 2I), and the coating layer is uniform with a thickness about 1 nm. The particle size distributions are in good agreement with the normal distribution (Figure 2J).

In order to investigate the induced magnetic anisotropy behavior of spherical Fe_3O_4 nanoparticles, the (APTS-Fe_3O_4/LDH)$_n$ films were fabricated through alternate deposition of the LDHs nanosheets and APTS-Fe_3O_4 nanoparticles on quartz substrates. Figure 3A shows the UV–vis absorption spectra of

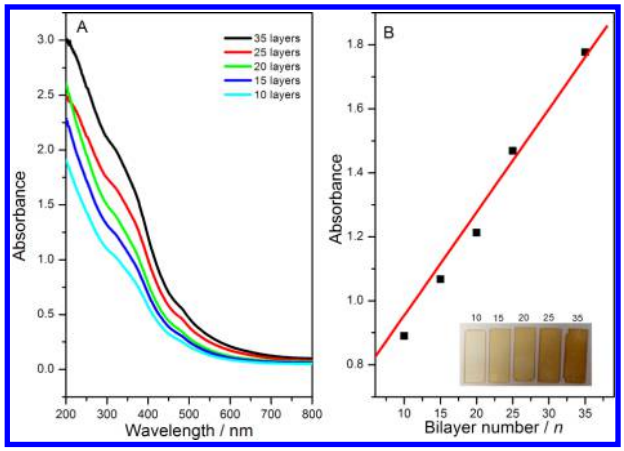

Figure 3. (A) UV–vis spectra of the (APTS-Fe_3O_4/LDH)$_n$ films (x = 3 and t = 0) with various bilayer numbers. (B) Absorption intensity as a function of bilayer number (inset: photographs).

the (APTS-Fe_3O_4/LDH)$_n$ films (x = 3 and t = 0, t stands for exfoliating time of LDH nanosheets) with n indicating different number of bilayers. Although no obvious absorption peaks of Fe_3O_4 were observed, the absorption intensity of the films across the whole spectrum range gradually increases with the increase of the number of bilayers. The absorption intensity at ~350 nm correlates linearly with n (Figure 3B), indicating a stepwise and regular film growth procedure. In the cases where $x \neq 3$, similar phenomena are also observed (not shown here). This was further confirmed by the gradual color enhancement

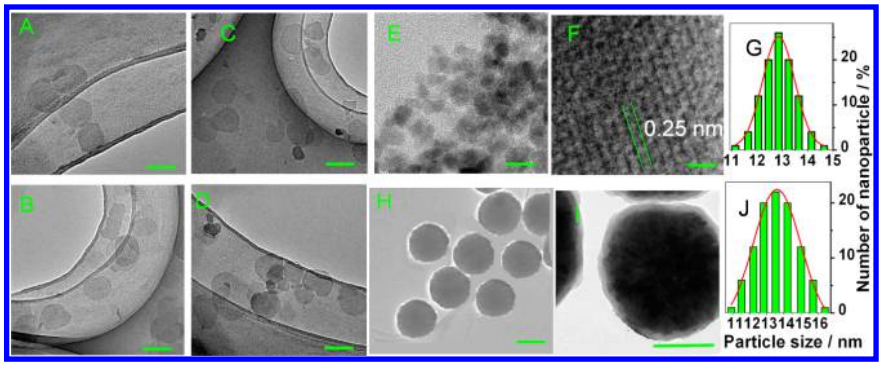

Figure 2. (A–D) TEM images of the Mg_xAl-LDHs (x = 1, 2, 3, and 4, scale bar = 100 nm). (E) HRTEM image of Fe_3O_4 nanoparticles at low magnification (scale bar = 10 nm), (F) same high-magnification (scale bar = 0.5 nm). (G) Particle size distribution of the Fe_3O_4 nanoparticles. (H) HRTEM image of APTS-Fe_3O_4 nanoparticles low magnification (scale bar = 10 nm), (I) same at high magnification (scale bar = 0.5 nm). (J) Particle size distributions of APTS-Fe_3O_4 nanoparticles.

DOI: 10.1021/acs.jpcc.5b01065
J. Phys. Chem. C 2015, 119, 13215–13223

with the increase of bilayer number (inset in Figure 3B). The surface morphology of the $(APTS\text{-}Fe_3O_4/LDH)_{10}$ (x = 3 and t = 0 h) film was characterized by SEM and AFM images. SEM image (Figure 4A) of the film from a top view shows that the

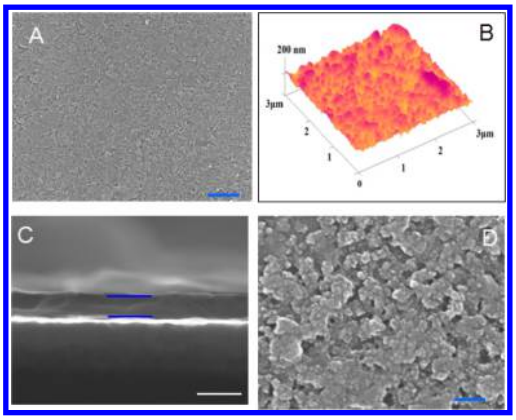

Figure 4. $(APTS\text{-}Fe_3O_4/LDH)_{10}$ film (x = 3 and t = 0 h) (A) Top view SEM image of the film (scale bar = 2 μm). (B) AFM image. (C) side view SEM image (scale bar = 500 nm). Blue markers indicate the bottom and top of the film. (D) high-magnification SEM image (scale bar = 200 nm).

film surface is continuous and uniform, with a root-mean-square (RMS) roughness of ~15.8 nm (Figure 4B). The film thickness is around 300 nm (Figure 4C), from which the thickness of one bilayer $(APTS\text{-}Fe_3O_4/LDH)_1$ (x = 3 and t = 0 h) was estimated to be ~30 nm. According to the thickness of ~15 nm for an LDH nanosheet and the diameter of ~14 nm for an $APTS\text{-}Fe_3O_4$ nanoparticle, $APTS\text{-}Fe_3O_4$/LDH supramolecular structure demonstrates the ideal single-layered arrangement model (Figure 5). The film thickness approximately linear increases as a function of bilayer number, confirming a uniform and periodic layered structure (Figure S2). A high-magnification SEM image ($APTS\text{-}Fe_3O_4$ as the terminal layer, Figure 4D) demonstrates the $APTS\text{-}Fe_3O_4$ nanoparticle is well-dispersed on the layer of LDH.

3.2. Magnetic Properties of the $(APTS\text{-}Fe_3O_4/LDH)_n$ Films. In order to obtain films with magnetic anisotropy we control the Fe_3O_4 interparticle spacing, in the horizontal and vertical directions and measure the magnetic properties (coercivity H_c and saturation magnetization M_s) of the $(APTS\text{-}Fe_3O_4/LDH)_n$ films. The main control tool, as discussed, are the charge density and layer thickness of LDH nanosheets.

3.2.1. Tuning of the Particle Density in the Horizontal Direction by Changing the Charge Density of the LDH Nanosheets. The tunability of positive charge density on the surface of the LDH nanosheets originates from their tunable metal ratio of bivalent and trivalent. This provides the chance of controlling dispersion degree and interparticle distance for $APTS\text{-}Fe_3O_4$ nanoparticles, which is absolutely critical for the purpose of tuning the magnetic property for collective films. The interaction of adjacent particles can be neglected when the interparticle distance is more than a critical value.[26] Therefore, in order to eliminate the interparticle interaction in vertical direction as far as possible, the unexfoliated LDH nanosheets with a maximum thickness of ~15 nm were used to assemble with spherical $APTS\text{-}Fe_3O_4$ nanoparticles and are shown in Figure 6.

The magnetic hysteresis loops for the Fe_3O_4, $APTS\text{-}Fe_3O_4$ nanoparticle (Figure S3), and the $(APTS\text{-}Fe_3O_4/LDH)_{35}$ films (x = 1, 2, 3, and 4, Figure 7) measured at room temperature are recorded. All of the samples exhibit the superparamagnetic behavior with negligible H_c (less than 14.0 Oe) and M_r (less than 0.90 emu g^{-1}).[27,28] The $(APTS\text{-}Fe_3O_4/LDH)_{35}$ films (x = 1, 2, 3, and 4) display noncoincident hysteresis loops in the parallel and perpendicular directions of magnetic field, compared to the coincident curves of the Fe_3O_4 and $APTS\text{-}Fe_3O_4$ nanoparticles, indicating magnetic anisotropy of films. The H_c value in the parallel direction is more than 3-folds higher than that in the perpendicular direction, but the M_s in the parallel direction is only ~80% of the perpendicular one (Table S1). This demonstrates that the rigid and oriented LDH nanosheets induce ordered alignment of the spherical Fe_3O_4 nanoparticles, resulting in magnetic anisotropy property of films. When magnetic fields are applied both parallel and perpendicular to the film, M_s increases at first and then decreases with further increase of x. The maximum values of 36.3 and 25.1 emu g^{-1} in perpendicular and parallel directions, respectively, are reached in the case of x = 3 due to excellent degree of dispersion and interparticle distance of $APTS\text{-}Fe_3O_4$ nanoparticles on LDH layer. This result indicates that the magnetic properties (H_c, M_s, and anisotropy) of films can be effectively controlled by changing the degree of dispersion and interparticle distance of $APTS\text{-}Fe_3O_4$ nanoparticles through simple tuning of the charge density of LDH layer. This can be explained by the "charge density-matching" assembly between the $APTS\text{-}Fe_3O_4$ nanoparticles and LDH nanosheets. In the case of $x \neq 3$, the charge density-mismatch may lead to the formation of aggregates (x = 1 and 2) and reduced stack density (x = 4) of $APTS\text{-}Fe_3O_4$ nanoparticles, consequently resulting in the decrease of M_s. Based on results above, particle shape is not the cause for the anisotropy of the $(APTS\text{-}Fe_3O_4/LDH)_{35}$ films (x = 1, 2, 3, and 4), since all the particles are spherical. Thus, the changes in anisotropy originate from the different dipolar interactions between NPs in the same layer. Moreover, it is noted that the M_s values for all of films in our work are lower than priviously reported values (80–90 emu g^{-1}),[29,30] which is caused by the lower content of pure Fe_3O_4 nanoparticle on the film. Therefore, the above results demonstrate that the magnetic properties of the assembled

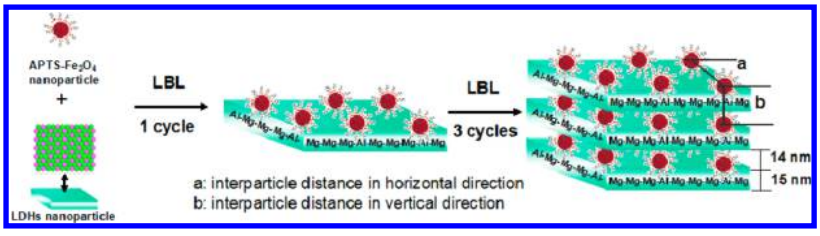

Figure 5. A schematic representation for the assembly and structure of the $(APTS\text{-}Fe_3O_4/LDH)_3$ film (x = 3 and t = 0 h).

DOI: 10.1021/acs.jpcc.5b01065
J. Phys. Chem. C 2015, 119, 13215–13223

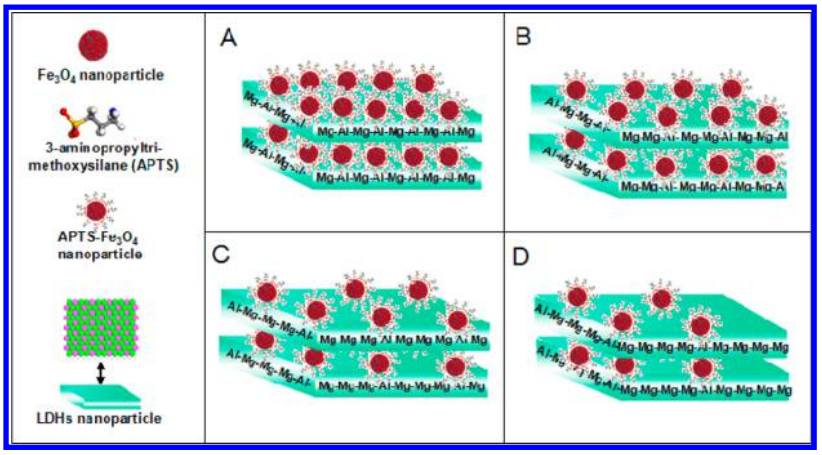

Figure 6. A schematic representation for the assembly and structure of the $(\text{APTS-Fe}_3\text{O}_4/\text{LDH})_2$ films and the effect of changing the composition (and charge) of the MgXAl-LDH material: (A) $x = 1$ and $t = 0$ h, (B) $x = 2$ and $t = 0$ h, (C) $x = 3$ and $t = 0$ h, and (D) $x = 4$ and $t = 0$ h.

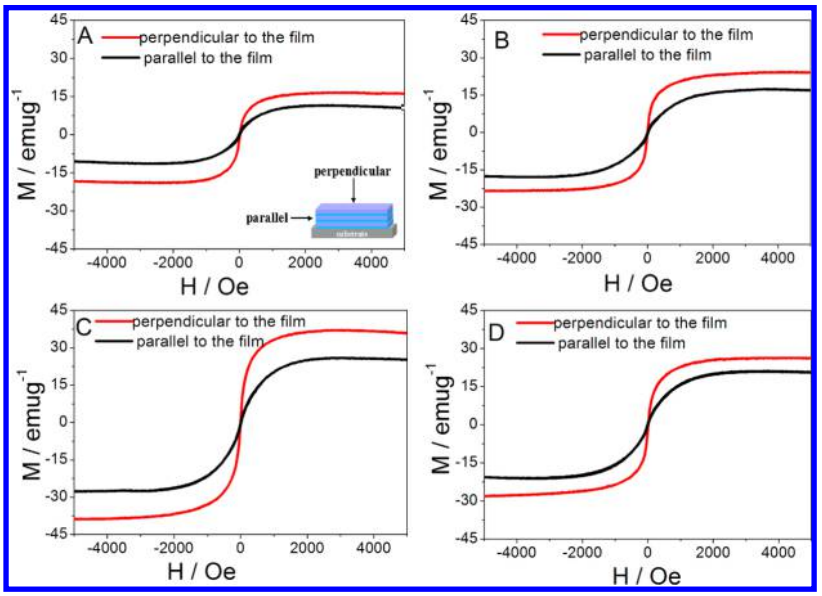

Figure 7. (A–D) Magnetic hysteresis loops of the $(\text{APTS-Fe}_3\text{O}_4/\text{LDH})_{35}$ films ($x = 1$, 2, 3, and 4, respectively), at room temperature.

films can be tuned by simply varying the charge density of the LDH layer. As Mg^{2+} and Al^{3+} can be mutually substituted in the LDH lattice, using non-integer x = Mg/Al ratios would allow precise tuning of the electrostatic charge on the surface.

The XPS measurment is used to explain the effect of charge density of LDH nanosheets on the magnetic property of $(\text{APTS-Fe}_3\text{O}_4/\text{LDH})_{35}$ films ($x = 1$, 2, 3, and 4) and is shown in Figure 8. Compared to the original APTS-Fe_3O_4 nanoparticles (NH_2: 399.2 eV, Figure 8A, curve a), the shift in the XPS peak of films for N 1s (NH_2: 398.7–398.1 eV, Figure 8A, curves b–e) to lower binding energy indicates APTS-Fe_3O_4 nanoparticles interact strongly with the LDH layers. The shift is monotonic, reaching a maximum in the film with $x = 3$ which we attribute to the best electrostatic charge match of LDH nanosheets to that of the APTS-Fe_3O_4 nanoparticles, and the interaction decreases again for $x = 4$. Similar shift is observed for the XPS peak of Fe $2p_{3/2}$ (from 711.5 eV of nanoparticle to 711.1–710.7 eV of films) and Fe $2p_{1/2}$ (from 725.1 eV of nanoparticle to 724.6–724.2 eV of films, Figure 8B), displaying the charge distribution of encapsulated Fe_3O_4 nanoparticles can also be affected by charge density out of APTS shell. Therefore, the tunable electrostatic interaction between LDH and APTS-Fe_3O_4 nanoparticles can be obtained by tuning x, which provides the tunability for the interparticle distance of Fe_3O_4 nanoparticles, leading to tunable magnetic properties. Though here we investigate only integer values of x, non-integer values of x are also possible (for $x < x_{max} = 4$), providing opportunities for fine control over the LDH surface charge.

3.2.2. Tuning of the Thickness of LDH Nanosheets for Particle Spacing in the Vertical Direction. Because of the multilayer feature of LDH, the originally synthesized LDH nanosheets can be further exfoliated to nanosheets with smaller thicknesses, which makes the tuning of the interparticle distance of Fe_3O_4 nanoparticles in vertical direction possible. Figure 9A shows the thickness of original LDH nanosheet is ~15 nm, which includes about 20 LDH single layers calculated by the ideal model (inset in Figure 9A). The Mg_3Al-LDHs sheets with a different thickness (~5, 10, and 15 nm) were obtained by exfoliating in formamide for different durations (t = 24, 5, and 0 h) before LBL assembly with APTS-Fe_3O_4 nanoparticles. The thickness of the $(\text{APTS-Fe}_3\text{O}_4/\text{LDH})_{10}$ films (t = 24, 5, and 0 h) is 200, 250, and 300 nm, respectively (Figure 9B–D). This is in agreement with the ideal single-layered arrangement model of the APTS-Fe_3O_4/LDH supra-

DOI: 10.1021/acs.jpcc.5b01065
J. Phys. Chem. C 2015, 119, 13215–13223

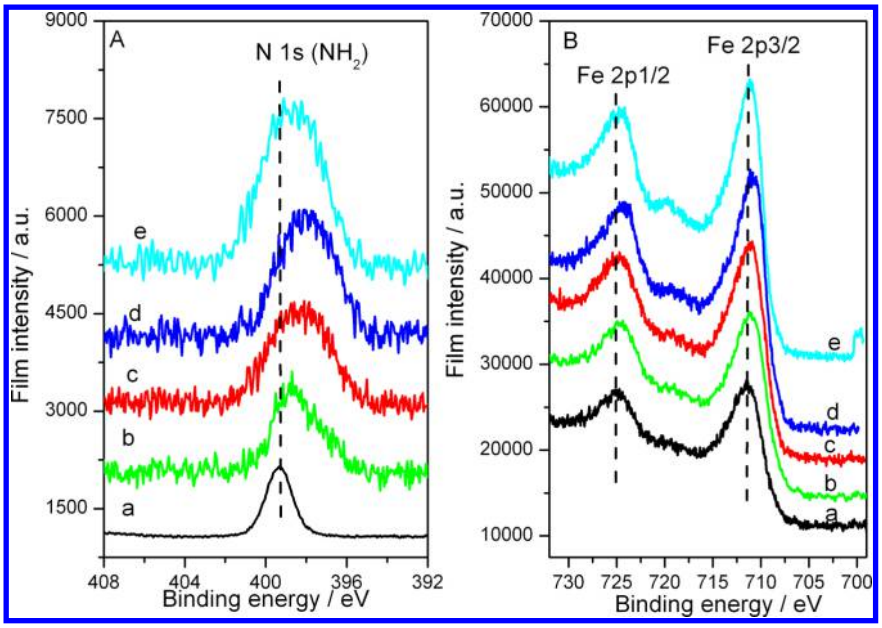

Figure 8. (A) N 1s and (B) Fe 2p XPS spectra of (a) APTS-Fe_3O_4 nanoparticles and (b–e) the $(APTS\text{-}Fe_3O_4/LDH)_{35}$ films (x = 1, 2, 3, and 4, respectively).

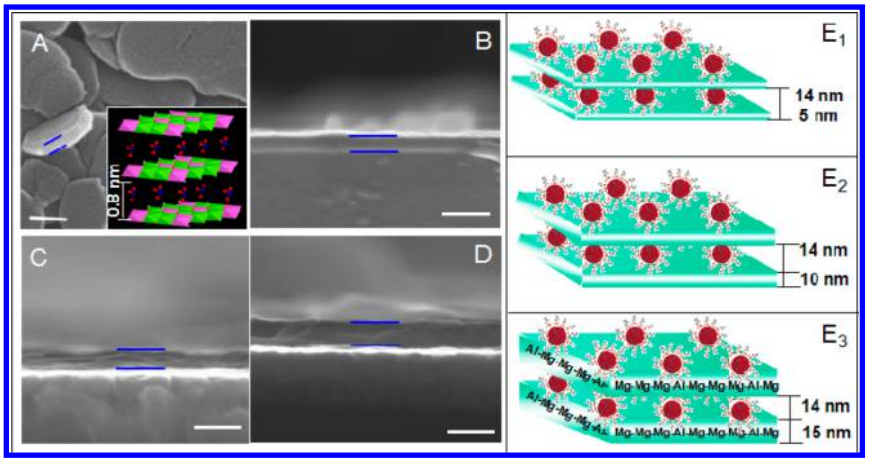

Figure 9. (A) Top view of SEM for unexfoliated Mg_3Al-LDHs nanosheets (inset: ideal model of LDH nanosheet, scale bar=30 nm). (B–D) Side view of SEM for the $(APTS\text{-}Fe_3O_4/LDH)_{10}$ films (x = 3, t = 24, 5, and 0 h, scale bar = 500 nm), respectively. (E) a representation for the structure of the $(APTS\text{-}Fe_3O_4/LDH)_2$ films: (E_1) x = 3 and t = 24 h, (E_2) x = 3 and t = 5 h, and (E_3) x = 3 and t = 0 h.

molecular structure with the thicknesses of ~5, 10, and 15 nm for different layers of LDH and ~14 nm for the spherical APTS-Fe_3O_4 nanoparticles (Figure 9E). Therefore, the interparticle distance of adjacent APTS-Fe_3O_4 nanoparticles in the vertical direction can be tuned by assembling with a different thickness of LDH nanosheets.

Generally, the interparticle spacing will have a great influence on the collective magnetic behavior, which can be observed from temperature-dependent ZFC/FC magnetization.[26] Thus, the ZFC/FC magnetization of the $(APTS\text{-}Fe_3O_4/LDH)_{10}$ films (x = 3, thickness of LDH layer is 0, 5, 10, 12, and 15 nm, respectively) has been tested at magnetic fields 10 Oe and shown in Figure 10. With increasing thickness (interparticle spacing in the vertical direction) of LDH layer, the maxima of the ZFC curves assigned to the mean blocking temperatures (T_B), as well as the splitting points (T_{irr}) between the ZFC and FC curves, shift toward lower temperatures. T_B decreased from 145 to 126 K as the interparticle spacing increased to 24 nm. A similar phenomenon was previously observed by García-Otero in dilute dispersed magnetic NPs.[31] Along further increasing interparticle spacing from 24 to 29 nm, no change of T_B is observed, displaying the disappearance of interparticles interaction. It is noted that this value (24 nm) is lower but similar to a previously reported value (31.5 nm),[26]perhaps reflecting the fact that for loosely-packed particles between LDH sheets, the interparticle spacing is larger than just accounting for the LDH layer thickness.

The magnetic properties of the $(APTS\text{-}Fe_3O_4/LDH)_{35}$ films (x = 3, t = 24, 5, and 0 h) were studied by measuring the magnetic hysteresis curves at room temperature (Figure 11A–C). The $(APTS\text{-}Fe_3O_4/LDH)_{35}$ films (x = 3, t = 24, 5, and 0 h) display apparent magnetic anisotropy. The H_c in the parallel direction is more than 4-folds than that in the perpendicular direction, but the M_s in parallel is less than 75% of perpendicular (Table S2). The maximum M_s is present in the assembly with the thickest LDH (t = 0) h with 29 nm particle distance in the vertical direction, which implies the absence of (or negligible) interparticle interactions for nanoparticles

DOI: 10.1021/acs.jpcc.5b01065
J. Phys. Chem. C 2015, 119, 13215–13223

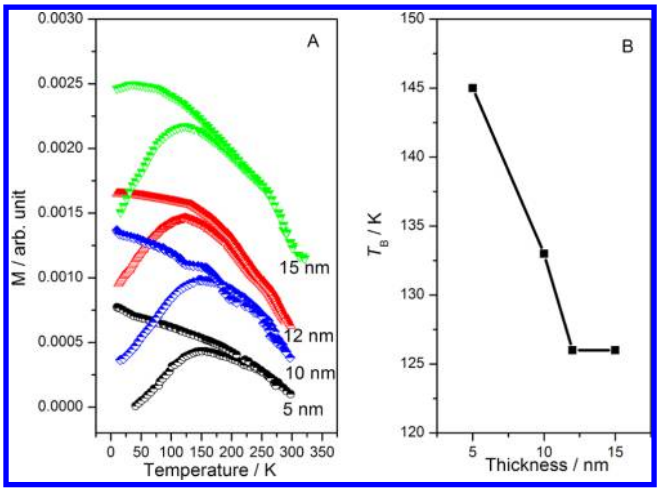

Figure 10. (A) FC (top) and ZFC (bottom) magnatization of the $(APTS\text{-}Fe_3O_4/LDH)_{10}$ films (x = 3, thickness of LDH layer = 5, 10, 12, and 15 nm, respectively). (B) T_B as a function of thickness of LDH layer.

spacing beyond 24 nm. In the case of smaller particle spacing of 14−24 nm, the $(APTS\text{-}Fe_3O_4/LDH)_{35}$ films (x = 3, t = 24 and 5) can be referred to as a coupled particles system. This result shows interparticle spacing of Fe_3O_4 has an effect on the collective magnetic behavior of the films, demonstrating the tunable magnetic anisotropy can be achieved by simply controlling the thickness of LDH nanosheets.

Raman spectra were measured to illustrate the effect of thickness change of LDH nanosheets on the magnetic property of the $(APTS\text{-}Fe_3O_4/LDH)_{35}$ films (x = 3, t = 24, 5, and 0 h). Figure 11D displays the Raman spectra of the Fe_3O_4, $APTS\text{-}Fe_3O_4$, and $(APTS\text{-}Fe_3O_4/LDH)_{35}$ films (x = 3, t = 24, 5, and 0 h) in the range 200−2000 cm^{-1}. The peak located at 670 cm^{-1} can be assigned to the A_{1g} mode of Fe_3O_4 (curve a).[32−35] After modifying by APTS molecules, the $APTS\text{-}Fe_3O_4$ spectra show two new peaks at 1336 cm^{-1} (τ CH_2 and ω CH_2) and 1564 cm^{-1} (δ NH_2) correspond to the APTS molecule, and indicating successful coating of APTS on the Fe_3O_4 (curve b). For the $(APTS\text{-}Fe_3O_4/LDH)_{35}$ films (x = 3, t = 24, 5, and 0 h), the blue-shift (from 670 to 645 cm^{-1}) and reduced peak intensity compared to $APTS\text{-}Fe_3O_4$ indicate that the intramolecular mobility (collisions, vibrations, and rotations, etc.) of Fe_3O_4 is decreased. This result is caused by the host−guest-like interactions and the influence of changed charge density of LDH layer. Moreover, the gradually increased blue-shift (from 659 to 622 cm^{-1}) and decreased intensity with increase of the thickness of LDH nanosheets (from 5 to 15 nm) demonstrate the increased immobilization and confining force of LDH nanosheet for Fe_3O_4 nanoparticles. Therefore, LDH layer induces the ordered and oriented stack of Fe_3O_4 nanoparticles in the interlayer of the LDH gallery, which imparts the anisotropic magnetic behavior for the films.

4. CONCLUSION

In summary, the $APTS\text{-}Fe_3O_4/LDH$ films with high anisotropy and tunable magnetic properties were obtained by alternate assembly of LDH nanosheets and spherical $APTS\text{-}Fe_3O_4$ nanoparticles through the layer-by-layer (LBL) method on a quartz substrate. The relationship between particle spacing (in the horizontal and vertical directions) of the Fe_3O_4 nanoparticles and magnetic properties of the $(APTS\text{-}Fe_3O_4/LDH)_n$ films is discussed from the viewpoint of charge density and layer thickness of the LDH nanosheets, respectively. The maximum saturation magnetization value is present in the sample of x=3 and t = 0 (M_s is 36.3 and 25.1 emu g^{-1} in perpendicular and parallel directions, respectively), which results from the excellent dispersion degree of $APTS\text{-}Fe_3O_4$ nanoparticles and charge density-matching assembly. XPS and Raman confirm that the electrostatic, immobilization, and confining forces between LDH and the $APTS\text{-}Fe_3O_4$ nanoparticles can be tuned. Both the interparticle distance of Fe_3O_4 nanoparticles and the magnetic anisotropy of the films can be controlled. The work also opens up possibilities for further

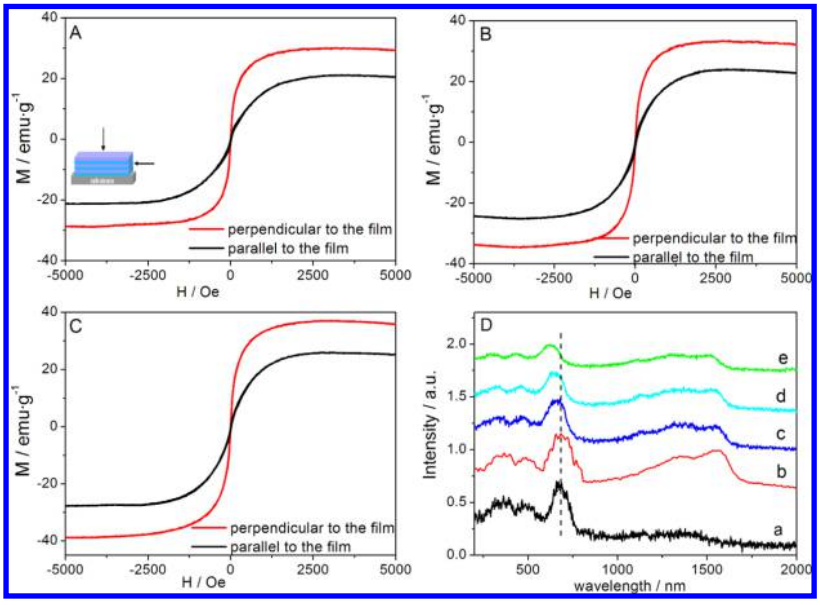

Figure 11. (A−C) Magnetic hysteresis loops of the $(APTS\text{-}Fe_3O_4/LDH)_{35}$ films (x = 3, t = 24, 5, and 0 h, respectively) at room temperature. (D) Raman spectra of (a) Fe_3O_4 nanoparticles, (b) $APTS\text{-}Fe_3O_4$ nanoparticles, and (c−e) the $(APTS\text{-}Fe_3O_4/LDH)_{35}$ films (x = 3, t = 24, 5, and 0 h, respectively).

DOI: 10.1021/acs.jpcc.5b01065
J. Phys. Chem. C 2015, 119, 13215−13223

control. By using washing/assembly solutions of higher pH, one could adjust the charge of the APTS-Fe_3O_4 NPs to more negative values. Similarly, ability to use non-integer ratios x = Mg/Al ratios in the LDH would allow finer control of the surface charge, and better optimization of both the spacing and magnetic properties. Therefore, this work not only provides a method to fabricate magnetic film with high anisotropy and tunability based on LDH nanosheets and APTS-Fe_3O_4 nanoparticles but also systematically deepens the understanding of the correlation between structure and magnetic anisotropic property of the APTS-Fe_3O_4/LDH films. According to this strategy, other anisotropy materials and devices can be obtained by virtue of inherent anisotropy of LDH nanosheets and the variety of functional molecules and nanoparticles.

■ ASSOCIATED CONTENT

Supporting Information

Magnetic parameters, SEM, and magnetic hysteresis loops. The Supporting Information is available free of charge on the ACS Publications website at DOI: 10.1021/acs.jpcc.5b01065.

■ AUTHOR INFORMATION

Corresponding Authors

*Ph +86-10-64412131; Fax +86-10-64425385; e-mail shiwy@mail.buct.edu.cn (W.Y.S.).

*Ph +44-01223-334435; Fax +44-01223-762088; e-mail sks46@cam.ac.uk (S.K.S.).

Notes

The authors declare no competing financial interest.

■ ACKNOWLEDGMENTS

This work was supported by the 973 Program (Grant 2014CB932103), the National Natural Science Foundation of China, the Scientific Research Foundation for the Overseas Chinese Scholars, and ERC grant EMATTER (#280078).

■ REFERENCES

(1) Matteo, M.; Pineider, F.; Sainctavit, P.; Danieli, C.; Otero, E.; Sciancalepore, C.; Talarico, A. M.; Arrio, M.-A.; Cornia, A.; Gatteschi, D.; et al. Magnetic Memory of a Single-Molecule Quantum Magnet Wired to a Gold Surface. *Nat. Mater.* **2009**, *8*, 194−197.

(2) Loth, S.; von Bergmann, K.; Ternes, M.; Otte, A. F.; Lutz, C. P.; Heinrich, A. J. Controlling the State of Quantum Spins with Electric Currents. *Nat. Phys.* **2010**, *6*, 340−344.

(3) Leuenberger, M. N.; Loss, D. Quantum Computing in Molecular Magnets. *Nature* **2001**, *410*, 789−793.

(4) Tejada, J.; Chudnovsky, E. M.; del Barco, E.; Hernandez, J. M.; Spiller, T. P. Magnetic Qubits as Hardware for Quantum Computers. *Nanotechnology* **2001**, *12*, 181−186.

(5) Urban, J. J.; Talapin, D. V.; Shevchenko, E. V.; Murray, C. B. Self-Assembly of PbTe Quantum Dots into Nanocrystal Superlattices and Glassy Films. *J. Am. Chem. Soc.* **2006**, *128*, 3248−3255.

(6) Petit, C.; Russier, V.; Pileni, M. P. Effect of the Structure of Cobalt Nanocrystal Organization on the Collective Magnetic Properties. *J. Phys. Chem. B* **2003**, *107*, 10333−10336.

(7) Puntes, V. F.; Gorostiza, P.; Aruguete, D. M.; Bastus, N. G.; Alivisatos, A. P. Collective Behaviour in Two-Dimensional Cobalt Nanoparticle Assemblies Observed by Magnetic Force Microscopy. *Nat. Mater.* **2004**, *3*, 263−268.

(8) Sun, S.; Anders, S.; Thomson, T.; Baglin, J. E. E.; Toney, M. F.; Hamann, H. F.; Murray, C. B.; Terris, B. D. Controlled Synthesis and Assembly of FePt Nanoparticles. *J. Phys. Chem. B* **2003**, *107*, 5419−5425.

(9) Duong, B.; Khurshid, H.; Gangopadhyay, P.; Devkota, J.; Stojak, K.; Srikanth, H.; Tetard, L.; Norwood, R. A.; Peyghambarian, N.; Phan, M.-H.; et al. Enhanced Magnetism in Highly Ordered Magnetite Nanoparticle-Filled Nanohole Arrays. *Small* **2014**, *10*, 2840−2848.

(10) Mamedov, A.; Ostrander, J.; Aliev, F.; Kotov, N. A. Stratified Assemblies of Magnetite Nanoparticles and Montmorillonite Prepared by the Layer-by-Layer Assembly. *Langmuir* **2000**, *16*, 3941−3949.

(11) Mamedov, A. A.; Kotov, N. A. Free-Standing Layer-by-Layer Assembled Films of Magnetite Nanoparticles. *Langmuir* **2000**, *16*, 5530−5533.

(12) Gorin, D.; Sukhorukov, G. B.; Yashchenok, A.; Maltseva, E.; Möhwald, H. Polyelectrolyte/magnetite Nanoparticle Multilayers: Preparation and Structure Characterization. *Langmuir* **2007**, *23*, 12388−12396.

(13) Paterno, L. G.; Soler, M. A. G.; Fonseca, F. J.; Sinnecker, J. P.; Sinneker, E. H. C. P.; Lima, E. C. D.; Novak, M. A.; Morais, P. C. Layer-by-Layer Assembly of Bifunctional Nanofilms: Surface-Functionalized Maghemite Hosted in Polyaniline. *J. Phys. Chem. C* **2009**, *113*, 5087−5095.

(14) Pichon, B. P.; Louet, P.; Felix, O.; Drillon, M.; Begin-Colin, S.; Decher, G. Magnetotunable Hybrid Films of Stratified Iron Oxide Nanoparticles Assembled by the Layer-by-Layer Technique. *Chem. Mater.* **2011**, *23*, 3668−3675.

(15) Shi, W. Y.; Wei, M.; Lu, J.; Li, F.; He, J.; Evans, D. G.; Duan, X. Molecular Orientation and Fluorescence Studies on Naphthalene Acetate Intercalated Zn_2Al Layered Double Hydroxide. *J. Phys. Chem. C* **2008**, *112*, 19886−19895.

(16) Yan, D. P.; Lu, J.; Ma, J.; Wei, M.; Li, S. D.; Evans, D. G.; Duan, X. Near-Infrared Absorption and Polarized Luminescent Ultrathin Films Based on Sulfonated Cyanines and Layered Double Hydroxide. *J. Phys. Chem. C* **2011**, *115*, 7939−7946.

(17) Yan, D.; Lu, J.; Wei, M.; Ma, J.; Evans, D. G.; Duan, X. Layer-by-Layer Assembly of Ruthenium(II) Complex Anion/Layered Double Hydroxide Ordered Ultrathin Films with Polarized Luminescence. *Chem. Commun.* **2009**, *45*, 6358−6360.

(18) Li, S. D.; Lu, J.; Ma, H. K.; Yan, D. P.; Li, Z.; Qin, S. H.; Evans, D. G.; Duan, X. Luminous Ultrathin Films by the Ordered Micellar Assembly of Neutral Bis(8-hydroxyquinolate)zinc with Layered Double Hydroxides. *J. Phys. Chem. C* **2012**, *116*, 12836−12843.

(19) Sudeshna, C.; Shailee, M.; Saumya, N.; Bahadur, D. Transformation, Memorization and Amplification of Chirality in Cationic Co(III) Complex−Porphyrin Aggregates. *New J. Chem.* **2010**, *34*, 1394−1400.

(20) Pan, B. F.; Gao, F.; Ao, L. M. Investigation of Interactions between Dendrimer-Coated Magnetite Nanoparticles and Bovine Serum Albumin. *J. Magn. Magn. Mater.* **2005**, *293*, 252−258.

(21) Pan, B. F.; Cui, D.; Gao, F.; He, R. Growth of Multi-Amine Terminated Poly(amidoamine) Dendrimers on the Surface of Carbon Nanotubes. *Nanotechnology* **2006**, *17*, 2483−2489.

(22) Lu, Y.; Yin, Y.; Mayers, B. T.; Xia, Y. Y. Modifying the Surface Properties of Superparamagnetic Iron Oxide Nanoparticles through a Sol−Gel Approach. *Nano Lett.* **2002**, *2*, 183−186.

(23) Bontchev, P. P.; Liu, S.; Krumhansl, J. L.; Voigt, J. Synthesis, Characterization, and Ion Exchange Properties of Hydrotalcite $Mg_6Al_2(OH)_{16}(A)_x(A')_{2-x}\cdot 4H_2O$ (A, A′ = Cl^-, Br^-, I^-, and NO_3^-, $2 \geq x \geq 0$) Derivatives. *Chem. Mater.* **2003**, *15*, 3669−3675.

(24) Xing, Z. H.; Wang, S. S.; Xu, A. W. Dipole-directed Assembly of Fe_3O_4 Nanoparticles into Nanorings via Oriented Attachment. *CrystEngComm* **2014**, *16*, 1482−1487.

(25) Jiao, F.; Jumas, J.-C.; Womes, M.; Chadwick, A. V.; Harrison, A.; Bruce, P. G. Synthesis of Ordered Mesoporous Fe_3O_4 and γ-Fe_2O_3 with Crystalline Walls Using Post-Template Reduction/Oxidation. *J. Am. Chem. Soc.* **2006**, *128*, 12905−12909.

(26) Yang, H. T.; Hasegawa, D.; Takahashi, M.; Ogawa, T. Achieving a Noninteracting Magnetic Nanoparticle System through Direct Control of Interparticle Spacing. *Appl. Phys. Lett.* **2009**, *94*, 013103−3.

(27) Leslie-Pelecky, D. L.; Rieke, R. D. Magnetic Properties of Nanostructured Materials. *Chem. Mater.* **1996**, *8*, 1770−1783.

(28) Kim, J. Y.; Shin, D. H.; Ihn, K. J.; Nam, C. W. Synthesis of Magnetic Nanocomposite Based on Amphiphilic Polyurethane Network Films. *Macromol. Chem. Phys.* **2002**, *203*, 2454−2462.

DOI: 10.1021/acs.jpcc.5b01065
J. Phys. Chem. C 2015, 119, 13215−13223

(29) Sun, S. H.; Zeng, H. Size-Controlled Synthesis of Magnetite Nanoparticles. *J. Am. Chem. Soc.* **2002**, *124*, 8204−8205.
(30) Horechyy, A.; Zafeiropoulos, N. E.; Nandan, B.; Formanek, P.; Simon, F.; Kiriy, A.; Stamm, M. Highly Ordered Arrays of Magnetic Nanoparticles Prepared via Block Copolymer Assembly. *J. Mater. Chem.* **2010**, *20*, 7734−7741.
(31) García-Otero, J.; Parto, M.; Rivas, J.; Bunde, A. Influence of Dipolar Interaction on Magnetic Properties of Ultrafine Ferromagnetic Particles. *Phys. Rev. Lett.* **2000**, *84*, 167−170.
(32) Melendres, C. A.; Pankuch, M.; Li, Y. S.; Lnight, R. L. Surface Enhanced Raman Spectroelectrochemical Studies of the Corrosion Films on Iron and Chromium in Aqueous Solution Environments. *Electrochim. Acta* **1992**, *37*, 2747−2754.
(33) Xi, G.; Wang, C.; Wang, X. The Oriented Self-Assembly of Magnetic Fe_3O_4 Nanoparticles into Monodisperse Microspheres and Their Use as Substrates in the Formation of Fe_3O_4 Nanorods. *Eur. J. Inorg. Chem.* **2008**, *2008*, 425−431.
(34) Pinna, N.; Grancharov, S.; Beato, P.; Bonville, P. Magnetite Nanocrystals: Nonaqueous Synthesis, Characterization, and Solubility. *Chem. Mater.* **2005**, *17*, 3044−3049.
(35) Maslar, J. E.; Hurst, W. S.; Bowers, W. J.; Hendricks, J. H.; Aquino, M. I. In Situ Raman Spectroscopic Investigation of Aqueous Iron Corrosion at Elevated Temperatures and Pressures. *J. Electrochem. Soc.* **2000**, *147*, 2532−2542.

DOI: 10.1021/acs.jpcc.5b01065
J. Phys. Chem. C 2015, 119, 13215−13223